Liquid Crystals
Publication details, including instructions for authors and subscription information:
http://www.informaworld.com/smpp/title~content=t713926090

The synthesis and mesomorphic behaviour of tetracatenar di-hydrazine derivatives

Peng Zhang[a]; Songnan Qu[a]; Binglian Bai[a]; Haitao Wang[a]; Xia Ran[a]; Chengxiao Zhao[a]; Min Li[a]
[a] Key Laboratory of Automobile Materials, Ministry of Education, Institute of Materials Science and Engineering, Jilin University, Changchun, People's Republic of China

To cite this Article Zhang, Peng , Qu, Songnan , Bai, Binglian , Wang, Haitao , Ran, Xia , Zhao, Chengxiao and Li, Min(2009) 'The synthesis and mesomorphic behaviour of tetracatenar di-hydrazine derivatives', Liquid Crystals, 36: 8, 817 — 824
To link to this Article: DOI: 10.1080/02678290903063018
URL: http://dx.doi.org/10.1080/02678290903063018

Liquid Crystals,
Vol. 36, No. 8, August 2009, 817–824

Taylor & Francis
Taylor & Francis Group

The synthesis and mesomorphic behaviour of tetracatenar di-hydrazine derivatives

Peng Zhang, Songnan Qu, Binglian Bai, Haitao Wang, Xia Ran, Chengxiao Zhao and Min Li*

Key Laboratory of Automobile Materials, Ministry of Education, Institute of Materials Science and Engineering, Jilin University, Changchun 130012, People's Republic of China

(Received 24 March 2009; final form 25 May 2009)

Symmetrical four-chained (tetracatenar) di-hydrazine derivatives, namely oxalyl N',N'-bis(3,4-dialkoxybenzoyl)-hydrazide (BFH-*n*, *n* = 4, 6, 8, 10), were synthesised. Investigations on the liquid crystalline properties by differential scanning calorimetry (DSC), wide-angle X-ray diffraction (WAXD) and polarising optical microscopy (POM) showed that the di-hydrazine derivatives exhibited columnar mesophases and the symmetry of the mesophase changes from rectangular to hexagonal on increasing the temperature. The rectangular columnar mesophases of BFH-*n* (*n* = 6, 8, 10) remained stable down to 10°C during cooling and the subsequent recrystallisation from the Col_r phase of BFH-*n* (*n* = 6, 8, 10) was observed on the second heating runs. Furthermore, the average number of molecules packing in a column slice was estimated to be three, based on their X-ray diffraction results. Intermolecular hydrogen bonding between –C=O and –N–H groups in crystalline and liquid crystalline phases was confirmed.

Keywords: di-hydrazine derivatives; rectangular columnar phase; hexagonal columnar phase; polycatenar

1. Introduction

Polycatenar liquid crystals, which contain a long rod-like rigid core ending in two half-disc moieties, have attracted increasing attention because they could be considered as an intermediate situation between a rod-like and a disc-like molecule (*1–9*). In general, polycatenar liquid crystals showed nematic, smectic C, cubic, lamellar–columnar and columnar mesophases, depending on their molecular structure, such as the number and position of the terminal paraffinic chains, the core length and polar substituents (*1*, *2*). Since the last reviews on polycatenar liquid crystals published in 2002 (*2*), other interesting series of polycatenar mesogens have been described (*3–18*). For example, the first switchable columnar phase consisting of achiral bent-core polycatenar molecules was reported by Gorecka *et al.* (*3*). The columnar phase with column stratum built of few molecules, arranged in coplanar or conelike geometry, becomes axially polar with electric spontaneous polarisation reorientable in an electric field. Dipole and steric interactions were considered to be responsible for this unique packing (*3–5*). Furthermore, a series simple hexacatenar compound, being connected by intermolecular hydrogen bondings to form a columnar liquid crystalline phase, namely N,N'-bis(3,4,5-trialkoxylphenyl) ureas, was designed (*6*). Optoelectronic experiments and optical second harmonic generation interferometry were employed to confirm the polar order and the switching characteristics (*6*, *7*).

The intermolecular hydrogen bonding plays an important role in mesophase formation in the hydrazide derivatives (*19–22*). We have confirmed that lateral intermolecular hydrogen bonding was still interacting in the smectic A (SmA) phase and played an important role in stabilising the mesophase of the non-symmetric hydrazide derivatives (C*n*-NO2) (*23*). The presence of an intermolecular attractive force may enhance the parallel alignment and the combination of the lateral intermolecular interaction and the microphase segregation effect may be the leading contribution to the formation of the SmA phase. Furthermore, we have reported symmetric (N*n*) (*24*) and non-symmetric liquid crystal dimmers (E*m*C*n*) (*25*) containing hydrazide groups, where lateral intermolecular hydrogen bonding was demonstrated to be the driving force for the intercalated SmA phase. In our recent paper (*26*), twin-tapered di-hydrazine derivatives FH-T*n* (*n* = 6, 7, 8, 10) were reported to exhibit a hexagonal columnar phase and the intermolecular hydrogen bonding motif between the di-hydrazine groups, either in $CHCl_3$ at high concentration or in bulk, was confirmed.

In the present paper, as part of our continuing effort with these di-hydrazide derivatives, we report the synthesis, phase behaviour and the mesomorphic structures of symmetrical tetracatenar di-hydrazide derivatives, namely oxalyl *N'*,*N'*-bis(3,4-dialkoxybenzoyl)-hydrazide (BFH-*n*, *n* = 4, 6, 8, 10) (see Scheme 1). In the present case, the molecular shape of BFH-*n* is different from that of FH-T*n*, which showed a hexagonal columnar phase as reported in our recent paper (*26*). The effect of the length of the terminal alkoxy chains and the number of terminal chains on the phase behaviour was investigated.

*Corresponding author. Email: minli@mail.jlu.edu.cn

ISSN 0267-8292 print/ISSN 1366-5855 online

DOI: 10.1080/02678290903063018
http://www.informaworld.com

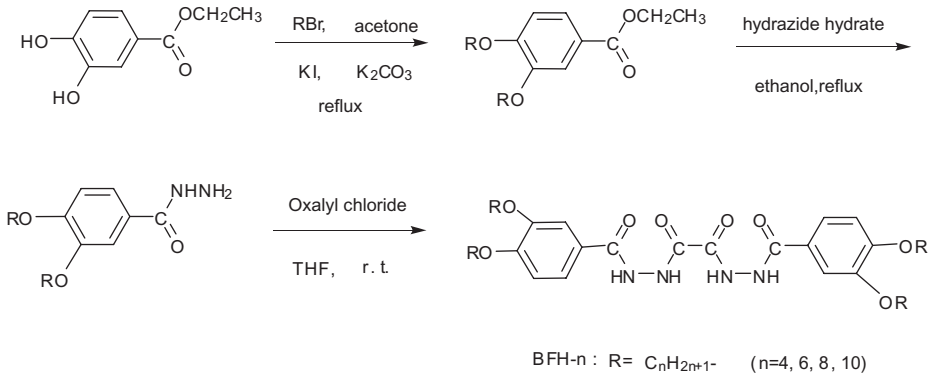

Scheme 1. Synthetic route for BFH-*n* compounds.

2. Experimental

2.1. Characterisation

^{1}H NMR spectra were recorded with a Mercury-300BB 300 MHz spectrometer, using tetramethylsilane (TMS) as an internal standard. Phase transitional properties were investigated with a Netzsch DSC 204. The rate of heating and cooling was 10°C min^{-1}. The weight of the sample was about 3 mg, and indium and zinc were used for calibration. The peak maximum was taken as the phase transition temperature. Texture observation was conducted on a Leica DMLP polarising optical microscope equipped with a Leitz 350 microscope heating stage. X-ray diffraction (XRD) was carried out with a Bruker Avance D8 X-ray diffractometer. Fourier transform infrared (FTIR) spectra were recorded with a Perkin-Elmer spectrometer (Spectrum One B); the sample was in the form of a pressed tablet with KBr.

2.2 Synthesis

The synthesis of BFH-*n* is similar to that of the hexacatenar analogues FH-T*n* and the detailed description of the synthesis and purification of the intermediate compounds can be found in our previous work (*26*). The crude products were further purified through recrystallisation from tetrahydrofuran (THF) for further nuclear magnetic resonance (NMR), FTIR spectroscopic measurements and elemental analysis. The yield was greater than 75%. (Because of poor solubility, the ^{1}H NMR measurement of BFH-8 and BFH-10 was not performed.)

Oxalyl *N*',*N*'-bis(3,4-dibutyloxybenzoyl)-hydrazide (BFH-4)

^{1}H NMR (300 MHz, DMSO), (ppm, from TMS): 10.77 (s, 2H); 10.34 (s, 2H); 7.53 (s, 2H); 7.49 (d, 2H, J = 3.3 Hz); 7.07 (d, 2H, J = 8.4 Hz); 4.03 (m, 8H); 1.71 (m, 8H); 1.46 (m, 8H); 0.95 (t, 12H, J = 7.2 Hz).

FTIR (KBr, pellet, cm^{-1}): 3202, 2957, 2872, 1671, 1612, 1577, 1514, 1451, 1416, 1389, 1341, 1302, 1274, 1233, 1130, 1065, 967, 853, 826, 780, 752, 724, 668, 639.

Elemental analysis: calculated for $C_{32}H_{46}N_4O_8$ (%), C, 62.52; H, 7.54; N, 9.11; Found, C, 62.50; H, 7.55; N, 9.16.

Oxalyl N',N'-bis(3,4-dihexyloxybenzoyl)-hydrazide (BFH-6)

^{1}H NMR (300 MHz, DMSO), (ppm, from TMS): 10.77 (s, 2H); 10.34 (s, 2H); 7.52 (s, 2H); 7.49 (d, 2H, J = 5.4 Hz); 7.06 (d, 2H, J = 8.4 Hz); 4.02 (m, 8H); 1.72 (m, 8H); 1.45 (m, 8H); 1.32 (m, 16H); 0.88 (t, 12H, J = 6.3 Hz).

FTIR (KBr, pellet, cm^{-1}): 3202, 2954, 2930, 2858, 1671, 1612, 1578, 1514, 1452, 1415, 1388, 1342, 1303, 1273, 1233, 1130, 1069, 965, 850, 827, 781, 753, 725, 669, 640.

Elemental analysis: calculated for $C_{40}H_{62}N_4O_8$ (%), C, 66.09; H, 8.60; N, 7.71; Found, C, 66.15; H, 8.62; N, 7.69.

Oxalyl N',N'-bis(3,4-dioctyloxybenzoyl)-hydrazide (BFH-8)

FTIR (KBr, pellet, cm^{-1}): 3199, 2923, 2853, 1671, 1611, 1578, 1515, 1454, 1415, 1388, 1342, 1304, 1272, 1229, 1130, 1068, 960, 850, 827, 782, 751, 723, 667, 640.

Elemental analysis: calculated for $C_{48}H_{78}N_4O_8$ (%), C, 68.70; H, 9.37; N, 6.68; Found, C, 68.64; H, 9.41; N, 6.73.

Oxalyl N',N'-bis(3,4-didecyloxybenzoyl)-hydrazide (BFH-10)

FTIR (KBr, pellet, cm^{-1}): 3195, 2955, 2921, 2851, 1671, 1611, 1576, 1515, 1454, 1415, 1389, 1342, 1304, 1274, 1229, 1130, 1067, 966, 850, 827, 782, 751, 723, 667, 640.

Elemental analysis: calculated for $C_{56}H_{94}N_4O_8$ (%), C, 70.70; H, 9.96; N, 5.98; Found, C, 70.87; H, 9.93; N, 5.94.

3. Results and discussion

3.1 Thermotropic mesomorphic behaviour of the BFH-n

The phase behaviour of BFH-*n* was studied by polarising optical microscopy (POM), differential scanning calorimetry (DSC) and WAXD. Figure 1 shows the DSC curves of BFH-*n* (n = 4, 6, 8, 10) in the first heating, the first cooling and the second heating cycles. Their transitional temperatures and associated enthalpies of BFH-*n* are summarised in Table 1. It can be seen that the phase behaviours were strongly affected by the length of the flexible terminal chains. BFH-4 showed two exothermic peaks at 218°C and 208°C, corresponding to the I–Col_r and Col_r–Cr transitions upon cooling from its isotropic phase, while there was one endothermic peak at 238°C, Corresponding to the Cr–I transition during heating. In contrast, higher homologues of BFH-*n* (n = 6, 8, 10) exhibited an enantiotropic Col_r and Col_h phase. It should be mentioned that no crystallisation was observed for the higher homologues of BFH-*n* (n = 6, 8, 10), even when they were cooled to 10°C at a cooling rate of 10°C min^{-1} (Figure 1(b)). BFH-10 showed two exothermic peaks at 238°C (7.28 kJ mol^{-1}) and 185°C (13.18 kJ mol^{-1}), corresponding to I–Col_h and Col_h–Col_r transitions upon cooling from the isotropic phase. Figure 2(a) shows the optical texture of BFH-10 in the Col_h phase on the cooling run (10°C min^{-1}).

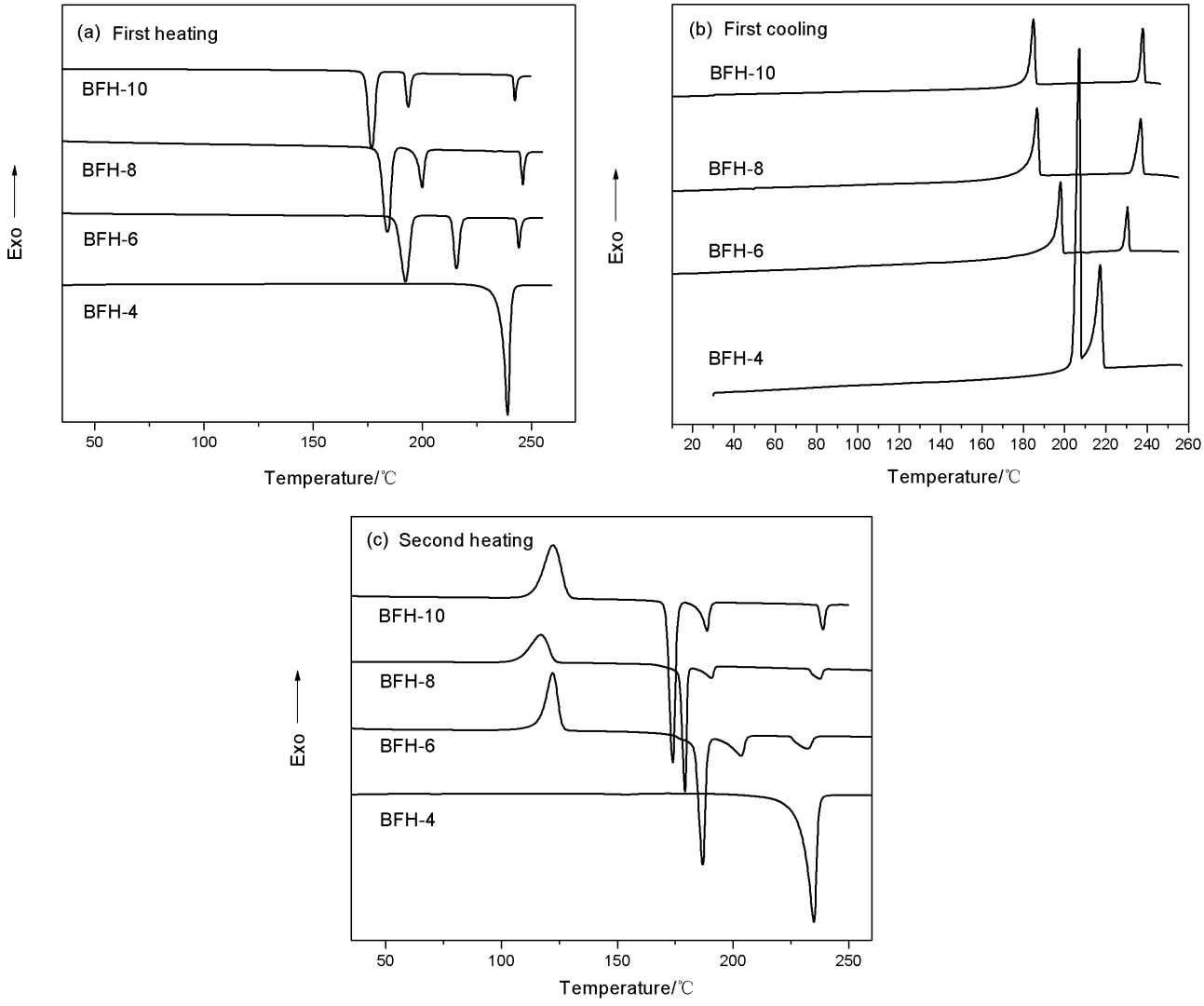

Figure 1. DSC curves of BFH-*n* (n = 4, 6, 8, 10): (a) on the first heating run; (b) on the cooling run; and (c) on the second heating run (10°C min^{-1}).

Table 1. Thermal transitional properties of BFH-*n*[a,b], transitional temperatures (°C) and the enthalpies of transition (kJ mol^{-1}, in parentheses).

Comp.	First heating	First cooling
BFH-4	Cr 238(62.14) I	I 218(17.92) Col_h 208(30.37) Cr
BFH-6	Cr 192(40.38) Col_r 215(20.25) Col_h 244(7.34) I	I 231(6.83) Col_h 198(13.04) Col_r
BFH-8	Cr 182(52.35) Col_r 198(17.43) Col_h 245(7.80) I	I 237(7.15) Col_h 187(14.63) Col_r
BFH-10	Cr 176(59.63) Col_r 193(16.63) Col_h 242(7.88) I	I 238(7.28) Col_h 185(13.18) Col_r

[a]Cr, Col_r, Col_h and I indicate crystalline state, rectangular columnar phase, hexagonal columnar phase and isotropic liquid, respectively.
[b]Scanning rate of 10°C min^{-1}.

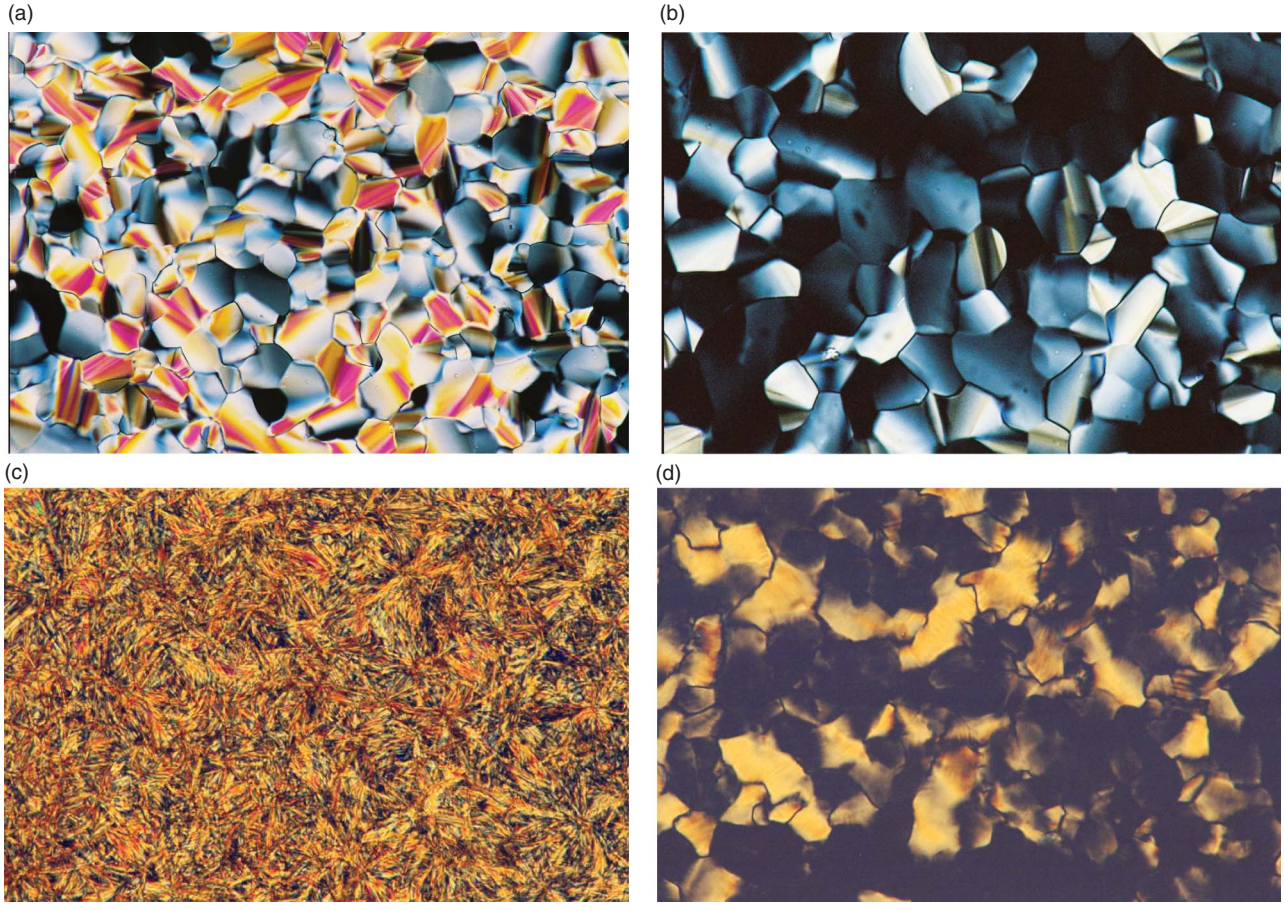

Figure 2. Optical textures observed for BFH-10 at: (a) 210°C (×400) on the cooling run; (b) 35°C (×400) on the first cooling run; (c) 148°C (×400) on the second heating run (10°C min^{-1}); (d) room temperature for more than 30 hours (×400).

The typically pseudo focal-conic texture with linear birefringent defects and the black areas, which are homeotropic domains with the columns aligned perpendicular to the glass substrates, suggested the characteristic of Col_h phases of BFH-10. Figure 2(b) shows the optical texture of BFH-10 at 35°C in its rectangular columnar phase, which was obtained through cooling from the Col_h phase and was stable up to 120°C during the second heating run. The Col_r feature of BFH-10 at 35°C was further confirmed by the XRD result (Figure 3(c)), which consists of two strong peaks at 29.8 Å (200) and 28.1 Å (110) in the small angle regions, as well as a diffuse halo centred at 4.5 Å.

BFH-10 showed one sharp exothermic peak centred at 122°C (55.05 kJ mol^{-1}) (Figure 1(c)) in the second heating run, which was assigned to recrystallisation from the Col_r phase. In addition, BFH-10 showed three endothermic peaks at 173°C (56.10 kJ mol^{-1}), 189°C (11.68 kJ mol^{-1}) and 239°C (6.69 kJ mol^{-1}), corresponding to Cr–Col_r, Col_r–Col_h and Col_h–I transitions,

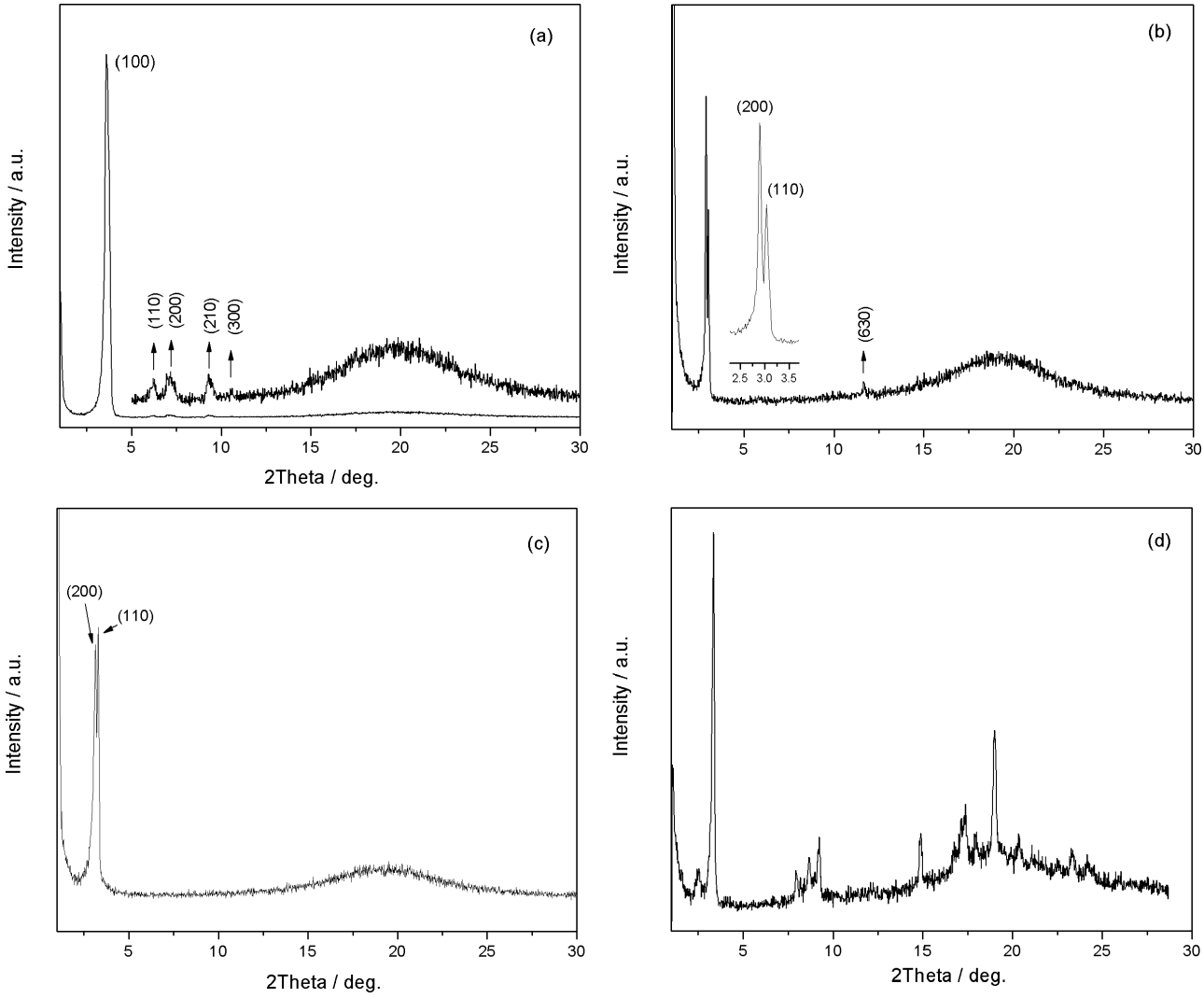

Figure 3. XRD patterns of: (a) BFH-6 at 235°C on the first heating run (10°C min^{-1}); (b) BFH-10 at 185°C on the first heating run (10°C min^{-1}); (c) BFH-10 at 35°C on the first cooling run; (d) BFH-10 at 150°C on the second heating run (10°C min^{-1}). The inset in (b) shows the Lorentzian fitted reflection peaks.

respectively. Considering the fact that both the temperatures and enthalpies in the second heating run are lower than those in the first heating run, we anticipated that BFH-*n* was unstable and thermal decomposition took place in the course of the heating and cooling cycles. Crystallisation from Col_r was observed under POM (Figure 2(c)), which showed pin-like morphology. Furthermore, crystallisation of the quenched Col_r phase of BFH-10 took place after being held at room temperature for more than 30 hours (Figure 2(d)). Figure 3(d) shows the XRD pattern for BFH-10 at 150°C on the second heating run (10°C min^{-1}), which consists of one strong peak in the low-angle region and several weak peaks in both the low- and high-angle regions, indicating the formation of a crystalline phase. Similar crystallisation phenomena were observed for the lower homologues of BFH-*n* ($n = 6, 8$). Thus, due to their slow crystallisation rate of BFH-*n* ($n = 6, 8, 10$), the Col_r phase could be quenched at room temperature.

In addition, the melting points descend, the transition enthalpies increase and thus the mesophase ranges broaden with the elongating of terminal chains. It may be understood that the incompatibility between the hydrogen-bonded rigid aromatic rings and flexible alkoxy chains increased, and thus the microphase segregation enhanced with the increase of length of the terminal chains. Such microsegregation effect was considered to be one of the driving forces for the formation of the columnar phase.

3.2 Intermolecular hydrogen bonding in BFH-n

Temperature-dependent FTIR spectroscopic experiments were performed to explore the hydrogen bonding

Table 2. Assignments of infrared frequencies for BFH-10 at room temperature.

Wavenumbers (cm^{-1})	Assignments
3195	ν (N–H)
2955, 2871	ν_{as} (CH_3), ν_s (CH_3)
2921, 2851	ν_{as} (CH_2), ν_s (CH_2)
1671, 1611	amide I,ν(C=O)
1576	ν(C=C) of phenyl ring
1515, 1229	Amide II,III, $\nu_{C\text{-}N}+\delta_{N\text{-}H}$
1454	δ_s (CH_2)
1389, 1342	CH_3 umbrella
1274	δ_{ip} (C–H) of phenyl ring
1130	ν (C–O)
850	δ(Ar–H)o.o.p, *para*-
723	$(CH_2)_n$ rocking vibration, $n \geq 4$

motif in BFH-*n*. Table 2 presents the assignments of infrared frequencies for BFH-10 at 25°C (*23*, *26*). The presence of N–H stretching vibrations at 3195 cm^{-1} (the absence of free N–H results in a relatively sharp peak with a frequency higher than 3400 cm^{-1}), the intense absorption of amide I at 1611 cm^{-1}, and the relatively weak absorption at 1671 cm^{-1} at 25°C indicated that almost all of the N–H groups are associated with C=O groups via N–H···O=C hydrogen bonding (*23*, *26–28*). Moreover, these conclusions were further supported by the fact that the N–H stretching vibration band and amide I bond became weaker and shifted to higher frequencies upon heating. The wavenumbers of ν(N–H) of BFH-10 are at around 3220, 3236, 3240 and 3300 cm^{-1} in the crystalline state, Col_r, Col_h and isotropic phase, respectively (Figure 4). The wavenumbers of the N–H stretching vibrations and amide I bond increased slightly in the crystalline state in the Col_r and

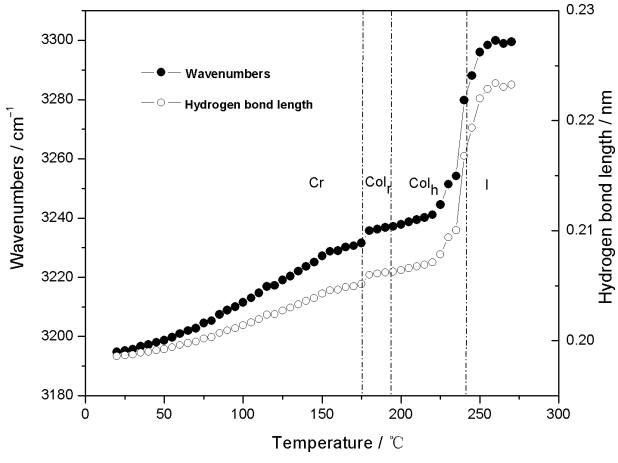

Figure 4. Temperature-dependent wavenumbers of N–H stretching vibrations of BFH-10.

Col_h phases, whereas the increase is significant in the isotropic phase with the increase of temperature, indicating that intermolecular hydrogen bonds still remained in the Col_r and Col_h phases, as well as in the isotropic state near the clearing point, although the average N–H···O=C distance is bigger than that in the crystalline state. The calculated hydrogen bonding length of N–H···O=C was 1.98 Å at 25°C, which is in the range of moderate hydrogen bonds (*29*, *30*). It increased slowly with temperature within the crystalline and columnar phases, while jumping to 2.23 Å, which indicated a weak hydrogen bonding, in the isotropic state (*29*). Considering the tremendous steric repulsion arising from the 3,4-dialkoxybenzoyl groups of the neighbouring molecules, the rotation of the phenyl rings away from the H-bonded bi-dihydrazine plane is necessary. Similar structures have already been reported for bi-dihydrazine polycatenar mesogens (*26*).

3.3 Mesophase structure of BFH-n

In order to get further information on molecular arrangements in their mesophases, variable temperature XRD was performed on BFH-*n*. The XRD patterns of BFH-6 at 235°C (Figure 3(a)) consists of one strong peak at 24.30 Å (100) and four weak peaks at 14.2 Å (110), 12.3 Å (200), 9.3 Å (210) and 8.3 Å (300) in the small angle regions, as well as a diffuse halo centred at 4.5 Å indicated the Col_h feature. Figure 3(b) shows the XRD pattern of BFH-10 at 185°C, in which two sharp peaks at 30.4 Å (200) and 28.5 Å (110), one weak peak at 7.6 Å and a broad, diffuse halo at about 4.5 Å were observed. Thus, the rectangular columnar mesophase of BFH-10 at 185°C was confirmed with the lattice parameter of a = 60.7 Å and b = 32.3 Å. Table 3 lists the *d*-spacings (Å) and the corresponding Miller indices of BFH-*n* (n = 4, 6, 8, 10) in the columnar phases.

According to the lattice parameters and the molecular structure, the average number of molecules (μ) in a column slice can be calculated through the equation $\mu = (N_A a_r b_r h\rho)/2M$ for the rectangular columnar phase and $\mu = (\sqrt{3}N_A a^2 h\rho)/2M$ for the hexagonal, where N_A is Avogadro's number, a_r, b_r and a are lattice parameters, h is the intracolumnar periodicity, ρ is the density (assumed to be 1 g cm^{-3}) and M is the molecular weight of the compound (*31*). The calculated average numbers of molecules (μ) are 2.7–2.9 (Table 3), e.g. there are approximately three BFH-*n* molecules within one columnar slice.

4. Conclusion

In summary, a new series of tetracatenar compounds containing a di-hydrazide central unit was synthesised.

Table 3. Powder WAXD results of BFH-*n* in the mesophases.

Compound	Mesophase	hkl	*d*, obsd (Å)	*d*, calcd (Å)	Lattice parameter (Å)	Molecules in a column slice (μ)	[a]Molecular length (ℓ)/Å
BFH-4	Col_h(212°C)	100	23.1 4.5 (halo)	23.1	a = 26.6	μ = 2.8	ℓ = 26.4
BFH-6	Col_r(208°C)	200	26.4	26.4	a = 52.8	μ = 2.9	ℓ = 30.9
		110	25.1 4.5 (halo)	25.1	b = 28.5		
	Col_h(235°C)	100	24.5	24.5	a = 28.3	μ = 2.7	
		110	14.2	14.1			
		200	12.3	12.2			
		210	9.3	9.2			
		300	8.3 4.5 (halo)	8.2			
BFH-8	Col_r(185°C)	200	28.2	28.2	a = 56.4	μ = 2.9	ℓ = 35.4
		110	26.8 4.5 (halo)	26.8	b = 30.4		
	Col_h(225°C)	100	26.9 4.5 (halo)	26.9	a = 31.0	μ = 2.8	
BFH-10	Col_r(185°C)	200	30.4	30.4	a = 60.7	μ = 2.9	ℓ = 40.0
		110	28.5	28.5	b = 32.3		
		630	7.6 4.5 (halo)	7.4			
	Col_h(230°C)	100	28.5	28.5	a = 32.9	μ = 2.7	
		200	14.3 4.5 (halo)	14.2			

[a]Molecular length was calculated by MM2.

BFH-4 exhibits a monotropic hexagonal columnar mesophase, while BFH-*n* (n = 6, 8, 10) showed both rectangular and hexagonal columnar phases. It was estimated that there were approximately three molecules (2.7–2.9, as calculated) in each columnar slice on average. BFH-*n* (n = 6, 8, 10) showed slow crystallisation during cooling from the isotropic melts. The microsegregation effect and intermolecular hydrogen bonding between the di-hydrazide groups played a crucial role in the formation of the columnar phase.

Acknowledgements

The authors are grateful to the National Science Foundation Committee of China (project No. 50373016, 50873044), the Program for New Century Excellent Talents in the Universities of China Ministry of Education, Special Foundation for PhD Program in the Universities of China Ministry of Education (Project No. 20050183057) and Project 985-Automotive Engineering of Jilin University for their financial support of this work.

References

(1) Nguyen, H.T.; Destrade, C.; Malthete, J. *Handbook of Liquid Crystals*, Demus, D., Goodby, J.W.; Gray, G.W.; Spiess, H.W. and Vill, V.; Wiley-VCH: Weinheim, 1998; Vol. 2B, ch 7.
(2) Gharbia, M.; Gharbi, A.; Nguyen, H.T.; Malthetec, J. *Curr. Opin. Colloid. Interface Sci.* **2002**, *7*, 312–325.
(3) Gorecka, E.; Pociecha, D.; Mieczkowski, J.; Matraszek, J.; Guillon, D.; Donnio, B. *J. Am. Chem. Soc.* **2004**, *126*, 15946–15947.
(4) Gorecka, E.; Pociecha, D.; Matraszek, J.; Mieczkowski, J.; Shimbo, Y.; Takanishi, Y.; Takezoe, H. *Phys. Rev. E* **2006**, *73*, 031704.
(5) Takezoe, H.; Kishikawa, K.; Gorecka, E. *J. Mater. Chem.* **2006**, *16*, 2412–2416.
(6) Kishikawa, K.; Nakahara, S.; Nishikawa, Y.; Kohmoto, S.; Yamamoto, M. *J. Am. Chem. Soc.* **2005**, *127*, 2565–2571.
(7) Okada, Y.; Matsumoto, S.; Takanishi, Y.; Ishikawa, K.; Nakahara, S.; Kishikawa, K.; Takezoe, H. *Phys. Rev. E* **2005**, *72*, 020701.
(8) Matraszek, J.; Mieczkowski, J.; Pociecha, D.; Gorecka, E.; Donnio, B.; Guillon, D. *Chem. Eur. J.* **2007**, *13*, 3377–3385.
(9) Eichhorn, S.H.; Paraskos, A.J.; Kishikawa, K.; Swager, T.M. *J. Am. Chem. Soc.* **2002**, *124*, 12742–12751.
(10) Plasseraud, L.; Cuervo, L.G.; Guillon, D.; Suss-Fink, G.; Deschenaux, R.; Brucea, D.W.; Donnio, B. *J. Mater. Chem.* **2002**, *12*, 2653–2658.
(11) Rais, K.; Daoud, M.; Gharbia, M.; Gharbi, A.; Nguyen, H.T. *Chem. Phys. Chem.* **2001**, *1*, 45–l49.
(12) Fazio, D.; Mongin, C.; Donnio, B.; Galerne, Y.; Guillonb, D.; Bruce, D.W. *J. Mater. Chem.* **2001**, *11*, 2852–2863.
(13) Ribeiro, A.C.; Heinrich, B.; Cruz, C.; Nguyen, H.T.; Diele, S.; Schroder, M.W.; Guillon, D. *Eur. Phys. J. E* **2003**, *10*, 143–151.
(14) Cardinaels, T.; Ramaekers, J.; Nockemann, P.; Driesen, K.; Hecke, K.V.; Meervelt, L.V.; Wang, G.J.; Feyter, S.D.; Iglesias, E.F.; Guillon, D.; Donnio, B.; Binnemansa, K.; Bruce, D.W. *Soft Matter* **2008**, *4*, 2172–2185.
(15) Wang, H.T.; Zhang, F.L.; Bai, B.L.; Zhang, P.; Shi, H.S.; Yu, D.Y.; Zhao, Y.F.; Wang, Y.; Li, M. *Liq. Cryst*. **2008**, *35*, 905–912.
(16) Seo, J.; Kim, S.; Gihm, S.H.; Park, C.R.; Park, S.Y. *J. Mater. Chem.* **2007**, *17*, 5052–5057.
(17) Yasuda, T.; Ooi, H.; Morita, J.; Akama, Y.; Minoura, K.; Funahashi, M.; Shimomura, T.; Kato, T. *Adv. Funct. Mater.* **2009**, *19*, 411–419.
(18) Yasuda, T.; Kishimoto, K.; Kato, T. *Chem. Commun.* **2006**, *32*, 3399–3401.

(19) Demus, D.; Gloza, A.; Hauser, H.; Rapthel, I.; Wiegeleben, A. *Cryst. Res. Technol.* **1981**, *16*, 1445–1451.
(20) Kutsumizu, S. *Curr. Opin. Solid St. Mater. Sci.* **2002**, *6*, 537–543.
(21) Beginn, U. *Prog. Polym. Sci.* **2003**, *28*, 1049–1105.
(22) Beginn, U.; Lattermann, G.; Festag, R.; Wendorff, J.H. *Acta Polym.* **1996**, *47*, 214–218.
(23) Pang, M.; Wang, H.T.; Li, M. *Tetrahedron* **2005**, *61*, 6108–6114.
(24) Wang, H.T.; Bai, B.L.; Zhang, P.; Long, B.H.; Tian, W.J.; Li, M. *Liq. Cryst*. **2006**, *33*, 445–450.
(25) Bai, B.L.; Wang, H.T.; Xin, H.; Shi, J.H.; Long, B.H.; Li, M. *J. Phys. Org. Chem.* **2007**, *20*, 589–593.
(26) Qu, S.N.; Li, F.; Wang, H.T.; Bai, B.L.; Xu, Y.X.; Zhao, L.J.; Long, B.H.; Li, M. *Chem. Mater.* **2007**, *19*, 4839–4846.
(27) Xue, C.; Jin, S.; Weng, X.; Ge, J.J.; Shen, Z.; Shen, H.; Graham, M.J.; Jeong, J.K.; Huang, H.; Zhang, D.; Guo, M.; Harris, F.W.; Cheng, S.Z.D. *Chem. Mater.* **2004**, *16*, 1014–1025.
(28) Shen, H.; Jeong, J.K.; Xiong, H.; Graham, M.J.; Leng, S.; Zheng, J.X.; Huang, H.; Guo, M.; Harris, F.W.; Cheng, S.Z.D. *Soft Matter* **2006**, *2*, 232–242.
(29) Steiner, T. *Angew. Chem. Int. Ed.* **2002**, *41*, 48–76.
(30) Rozenberg, M.; Loewenschuss, A.; Marcus, Y. *Phys. Chem. Chem. Phys.* **2000**, *2*, 2699–2702.
(31) Guillon, D. *Struct. Bonding* **1999**, *95*, 42–82.